HabEx Space Telescope Guiding Systems

Stefan Martin, Michael Bottom, Joel Nissen and Stuart Shaklan
Jet Propulsion Laboratory
California Institute of Technology
4800 Oak Grove Dr.
Pasadena, CA 91109
818-354-4605
stefan.r.martin@jpl.nasa.gov

Abstract— **The HabEx (Habitable Exoplanet Imaging Mission) study is developing concepts for a next generation space telescope operating from the ultraviolet to the infrared. HabEx is making exoplanet science the primary mission objective and adding two secondary payload instruments for general astrophysics, including ultraviolet spectroscopy. For exoplanet work, two approaches are being developed. The first is a coronagraph with two separate channels to cover a broad spectral range from 450 nm to 1000 nm in two observations. The second is a starshade to cover the band 300 nm to 1000 nm in a single observation. These instruments are complementary; the coronagraph can make rapid survey observations while the starshade can reach closer in to the star and once on target, enables more efficient spectroscopic observations. This paper describes some of the key design considerations necessary to enable coronagraph and starshade observations.**

TABLE OF CONTENTS

1. INTRODUCTION

The telescope, described in [1], is a three mirror anastigmat (TMA) with a 4 m diameter primary mirror, 2.5 m off axis, producing a collimated 50 mm beam at the output. Figure 1 shows a view of the telescope optics and Figure 2, the telescope instrument configuration. Each instrument has its own field of view on the sky (Figure 3). The collimated output greatly simplifies the accommodation of the instruments, since otherwise, off axis optics would be needed throughout the system. The primary mirror directs light to the off-axis secondary and thence to the tertiary. Instruments are arranged near the tertiary. In a three mirror design, the output beam is directed back towards the secondary mirror so that fold mirrors are normally employed to bring the beam back behind the tertiary mirror. In this design, a mirror placed between the tertiary and the exit pupil extracts the individual field so that it can be passed to an instrument. Since fields are separated on the tertiary, this allows different optical coatings on the tertiary to aid transmission efficiency in particular wavelength bands. A protected aluminum coating is required on at least the first two mirrors so that the telescope can operate down to a wavelength of 115 nm in the UV.

HabEx employs a wide field three mirror telescope design. For exoplanet studies, only a very narrow field of view is needed so that a simple Cassegrain or Ritchey-Chretien telescope could be considered, but since the general astrophysics (GA) instruments require 3'x3' fields of view, a design capable of producing a well-corrected wider field is needed. Also, a fine guidance sensor operating through the telescope aperture with a wide field of view is necessary to achieve sufficient roll and pointing stability when using the coronagraph. The large telescope aperture results in a small point spread function (PSF) ~20 mas in diameter. Pointing should then be readily controlled to about 2 mas for the general astrophysics (GA) instruments, but as will be seen, the coronagraph requires higher performance. Another guiding requirement is to navigate the starshade into position on the line of sight between the telescope and star, and maintain it in position within ±1 m. The process for achieving this will be described below. Alongside the fine pointing requirement for the telescope body, internal alignment of the telescope must also be maintained. This is achieved through a laser metrology truss that measures the distances between fiducials placed on the TMA mirrors to 0.15 nm rms accuracy. The metrology truss sensor signals control active devices that maintain the three mirrors in constant relative positions.

2. TELESCOPE INTERNAL STABILITY

Three telescope designs were modeled, two with a 4 m telescope aperture and one with a 6.5 m aperture. The two 4 m designs had magnifications of 40x and 80x (baseline), while the 6.5 m design had magnification of 65x. Each of the first three mirrors was displaced and rotated in 6 degrees of freedom and the output beam direction calculated, to obtain a budget to allocate alignment stability requirements. Table 1 shows an allocation of rigid body motions that reaches pointing accuracy ~2 mas rms. This allocation does not include an allocation for thermal or dynamic effects on the structure. A more detailed analysis is presented in [2]. Position and attitude ('pose') measurement coupled with active control of the optics is required to achieve such low

978-1-5386-2014-4/18/$31.00 ©2018 IEEE

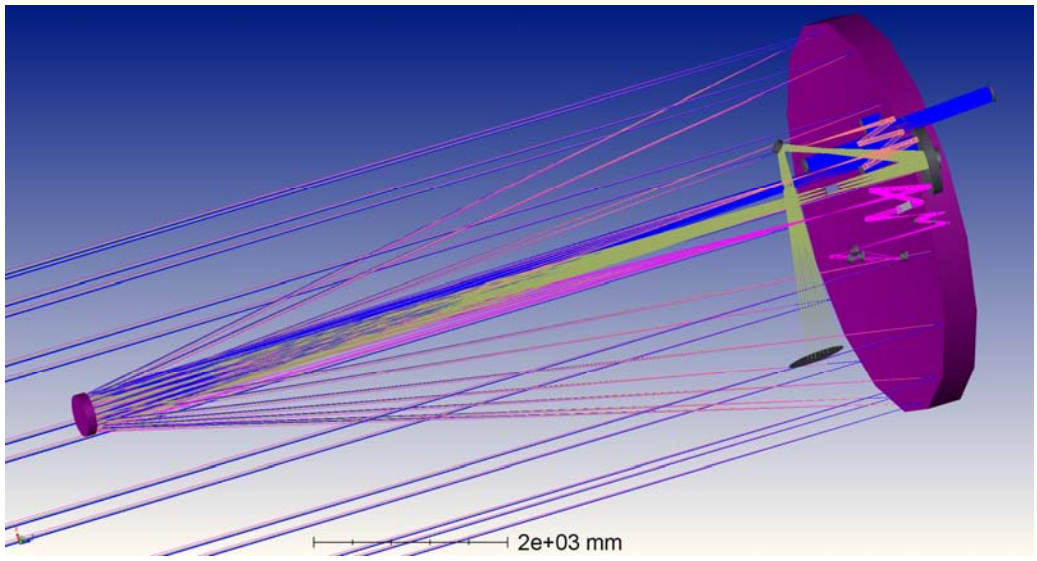

Figure 1: HabEx telescope optical system.

levels of position error. In a passive scenario, a low ($<10^{-6}$/K) coefficient of temperature expansion (CTE) telescope truss structure would be monitored by temperature sensors and maintained to the 1 mK level to preserve alignment. However, outgassing of a composite telescope structure causes continuous dimensional changes, so that such a scheme would not be reliable. To avoid this problem, a laser metrology truss is used to sense rigid body drift of the first three optics and then rigid body actuators are used to maintain alignment[3]. This system has other benefits too, such as the ability to hold the telescope setup precisely when moving between a bright star used to set up the deformable mirrors (DMs) and the target, or between target stars. The metrology truss (MET) is illustrated in Figure 4. A minimum of six distance measurements between the primary and secondary, and six distance measurements between secondary and tertiary mirrors are needed to control all twelve degrees of freedom for the primary and secondary mirrors. Six additional laser gauges are included to add redundancy. With an expected rms gauge error of 0.15 nm or better, the rms wavefront error will be less than 5 pm, keeping the contrast drift below 1×10^{-11} at 500 nm (80x telescope, based on contrast simulations analyzed using PROPER[4]).

Figure 5 shows the calculated coronagraph contrast (using the method of Shaklan et al. [5]) as a function of angle for the 40x, 80x and 65x designs utilizing vector vortexes of charges 6 and 8 as the coronagraphic mask. These contrasts were calculated for disturbances expected under an allocation budget consistent with Table 1. The target contrast for HabEx is 10^{-10}, and the contrast contributions from any source should be much less than this, $< \sim10^{-11}$ for example. All of these designs meet the requirement, but the charge 8 vortex improves considerably on the charge 6 vortex through its immunity to tip/tilt. Furthermore, the charge 8 vortex transmits little trefoil, which is commonly produced by three point mirror mounting schemes and is the major contributor

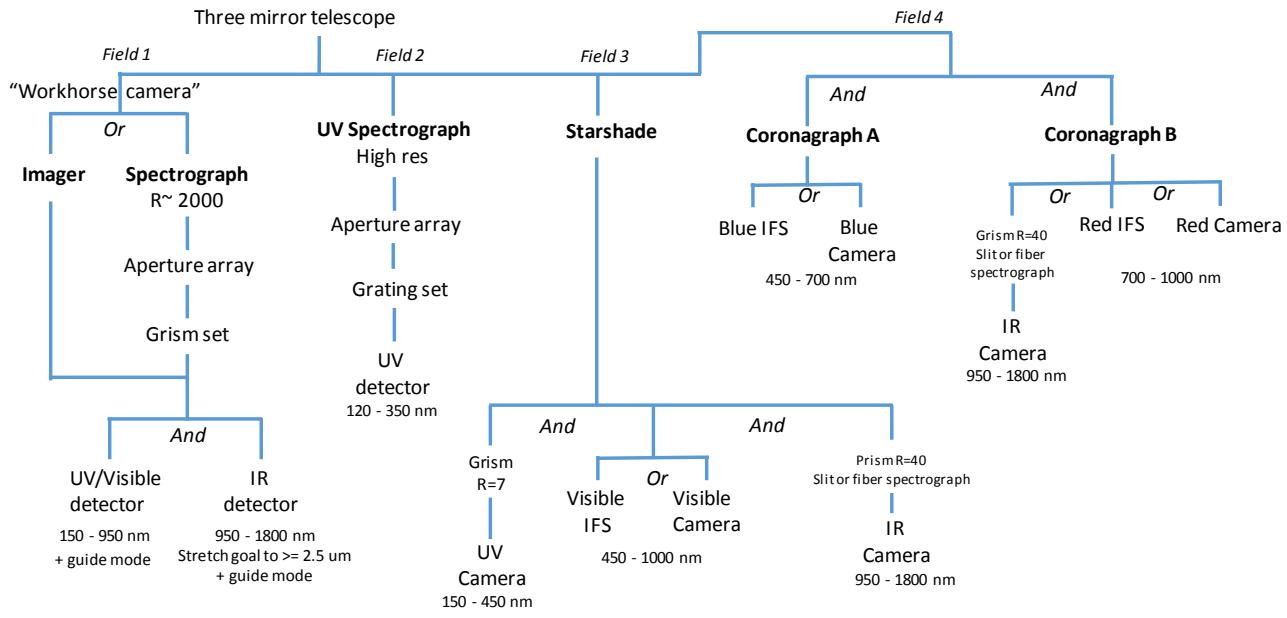

Figure 2: Optical instrument configuration.

Table 1: Allocated TMA optic motions that yield 2.2 and 2.4 mas on-sky for the 80x and 40x designs respectively. These allocations generate measurable metrology signals, enabling control of the telescope optics.

Optic	M1				M2				M3			
Move	DX,DY	DZ	TX,TY	TZ	DX,DY	DZ	TX,TY	TZ	DX,DY	DZ	TX,TY	TZ
Unit	nm	nm	nr	nr	nm	nm	nr	nr	nm	nm	nr	nr
Allocation	10	60	2.5	10	10	60	25	100	12	120	20	200
80x on-sky (mas)	0.2	0.3	1.0	0.5	0.2	0.3	0.9	0.4	0.0	0.0	0.1	0
40x on-sky (mas)	0.2	0.3	1.0	0.6	0.2	0.3	1.2	0.5	0	0	0.2	0
Met signal (nm)	4	117	9	9	1	120	10	1	1	240	12	3

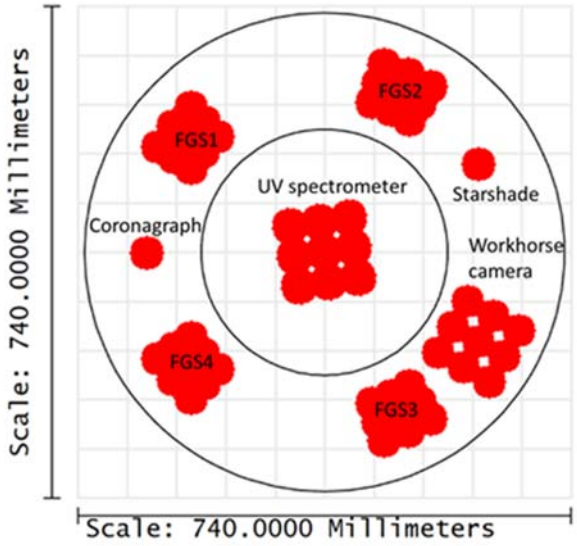

Figure 3: Instrument fields of view at the tertiary mirror (M3). The areas marked FGS are potential field area for the fine guidance sensors.

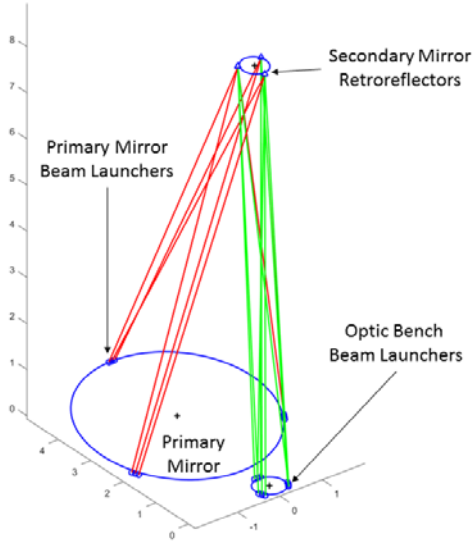

Figure 4: Layout of metrology truss. 'Optics bench' beam launchers are located on M3.

to contrast loss in the charge 6 case. As expected, the higher magnification telescopes have better contrast with the allocated disturbances because internal pointing changes on these telescopes translate to less pointing and therefore less wavefront error on the sky.

3. Telescope External Stability

Conventional star trackers are capable of pointing at the 100 mas level. Space telescopes such as Hubble require better pointing and employ a fine guidance sensor operating through the main telescope aperture in order to provide a small enough PSF for accurate guiding. The width of the PSF at 400 nm with the 4 m HabEx aperture is 100 nanoradian (~20 mas) FWHM. Assuming we need pointing to 1/10th the PSF diameter (suitable for GA and starshade instruments), then the desired accuracy is 2 mas (~10 nanoradian). Typically, pointing is measured on a CCD or quad cell sensor (except that Hubble uses an interferometric method [6]) and the nominal pointing accuracy for a single source is given by $FWHM$ of the PSF divided by $\sqrt{n}$ where n is the number of photons. Noise sources and the number of pixels covered by the PSF increase the required n (the typical need is ~140 e- to achieve an SNR of 10). On JWST, the fine guidance sensor [7] provides the data for fine pointing and attitude stabilization. Two channels image separate regions of sky onto independent 2048 × 2048 HgCdTe sensor chip arrays (SCAs). The field of view is 2.4' × 2.4' with a plate scale of 69 milliarcsec per pixel. The SCAs are responsive from 0.6 - 5 μm and provide the sensitivity to reach a J band magnitude of 18.6. The combination of sky coverage and sensitivity ensures that an appropriate guide star can be found with 95% probability at any point in the sky, including high galactic latitudes.

A similar configuration to JWST could be achieved on the HabEx telescope utilizing one of the GA instruments, the

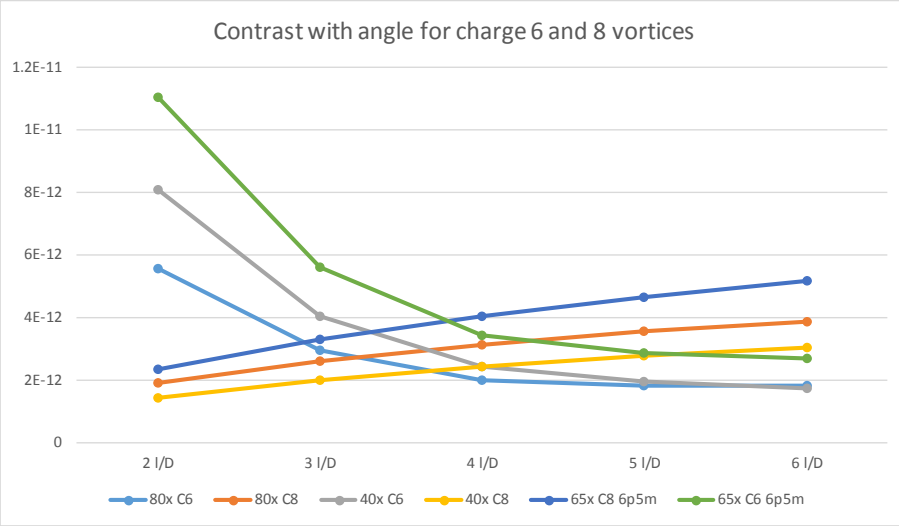

Figure 5: Calculated contrast for three telescope designs (80x, 40x and 65x, the 6.5 m design) using vector vortex coronagraphs of charge 6 and 8 (C6, C8) in the presence of alignment disturbances equivalent to the allocations shown in Table . The charge 8 vortex may be a good choice for HabEx despite its poor optical throughput at small inner working angles: note its comparative insensitivity to the tilt signal expected at small angles.

Workhorse Camera (WHC). This instrument has two channels which simultaneously observe the same field of view: an optical channel using delta-doped CCD detectors providing good throughput from ~150 nm to ~1 um, and a near-IR channel using HgCdTe arrays providing good throughput from ~950 nm to ~1.8 um, at which point thermal background dominates for most celestial targets. For good imaging, the pixel magnification is chosen to subsample the PSF at Nyquist frequency. To obtain the science field of view of 3'x3', the visible channel has a 3x3 array of 4k square CCD detectors, and the IR channel utilizes 2x2 H4RG10 (Teledyne detectors).

To estimate the effectiveness of the WHC for fine guiding we assume a 10 Hz closed loop on the body pointing, implying 100 Hz frame rate on the camera. At this rate, stellar magnitude of ~17 is adequate to reach an SNR of 10, which implies measurement accuracy of 1/10th the PSF diameter. 'Sharpness' [8] (1/number of pixels covered by the PSF, matched filtering assumed) of 0.1 was assumed and taking published data for the detectors, the required source brightness was calculated. Table 2 shows the results. The quoted stellar guide star takes into account read noise, dark current, pixels in PSF, QE, transmission of the optical system and frame rate. It is assumed that 3 stars are needed to provide tip/tilt and rotation sensitivity.

As can be seen in the table, on the visible detector, the EMCCD (electron multiplying CCD) does best and would provide about 97% sky coverage. (Sky coverage is estimated from a global average star density formula [9] number per square degree = 10^(-0.0003 M^3+ 0.0019 M^2 + 0.484 M - 3.82)). Thus, for the EMCCD visible detector, good sky coverage is obtained with a modest 200 nm optical bandwidth while for the infrared channel, a full 1000 nm bandwidth is needed. The LMAPD (Linear Mode Avalanche Photo Diode) detector shown in the table is not baselined for HabEx because of its relatively small area, but is an avalanche device under development that shows promise as an infrared detector with low read noise.

4. Fine Guiding Requirements

The coronagraph is very sensitive to wavefront changes. Initially, wavefront error introduced by the optical system is corrected on two deformable mirrors (DMs) included in the coronagraph beam train. During observations which may take many hours, the wavefront slowly evolves under small

Table 2: Required guide star magnitudes to reach an SNR of 10 with possible WHC detectors.

	Trans-mission	BW	Flux Photon/s	Read noise	Dark current	Magnitude	# stars in WHC FOV	Probability of having 3 stars in FOV
CCD	29%	600-800 nm	2.9e9	2	.000833	16.9	7.1	92%
EMCCD	29%	600-800 nm	2.9e9	0.26	0.01 ?	17.2	8.7	97%
sCMOS	29%	600-800 nm	2.9e9	2.3	0.15	16.8	6.7	90%
H4RG10	40%	1000-1200 nm	1.9e9	10	0.01	15.7	3	36%
LMAPD	40%	1000-1200 nm	1.9e9	2.3	0.15	16.7	6.2	87%
H4RG10	40%	800-1800 nm	7.8e9	10	0.01	17.2	8.7	97%
LMAPD	40%	800-1800 nm	7.8e9	2.3	0.15	18.3	17.1	100%

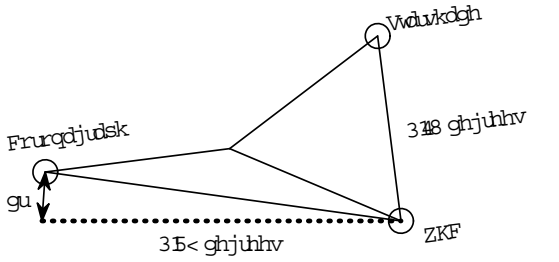

Figure 6: Geometry of workhorse camera, starshade instrument and coronagraph showing the centers of the fields of view arrayed on a 0.3° diameter circle.

thermal changes and will be detected on a low order wavefront sensor [10] (LOWFS), part of the coronagraph beam train. This sensor allows detection of the wavefront error at sub mas levels, so that tip/tilt can be corrected by the fine steering mirror (FSM) at the entrance to the coronagraph. Higher order errors can be corrected directly on the DMs.

Each instrument in the HabEx telescope has its own field of view, as seen in Figure 3 which shows the beam footprints on the tertiary mirror. Assuming the WHC is used for fine guiding, there is a separation of 0.29° between its field of view (FOV) and the coronagraph FOV. Figure 6 shows the geometry. Assume the telescope rotates around the center of the WHC FOV, then there is an induced motion of the coronagraph FOV on the sky, which appears as a tilt of the wavefront from the observed object. This tilt will be detected by the coronagraph LOWFS and corrected by the FSM. However, a residual wavefront error remains, caused principally by the beam footprint moving a small amount across the tertiary and the succeeding fold mirrors. Different parts of these mirrors have different residual surface irregularities, and the effect is to introduce an uncorrected wavefront error at the coronagraph input.

Angular accuracy of WHC

We select three guide stars more than 1 arc minute from center of WHC detector. To do this, the WHC detector plane is divided into 4 areas: a central region which is excluded, and 3 areas where a guide star must be found, see Figure 7. At 17th magnitude (M17), there is only ~53% probability of having 3 separated guide stars on the outer area, but at M~19 the probability rises to 98% (Figure 7, right). This magnitude would be compatible with a 10 Hz frame rate, implying that the innate telescope pointing jitter would be only at low frequency. For HabEx, the telescope will use microthrusters [11] rather than reaction wheels for attitude control. While reaction wheels typically produce jitter at frequencies in the hundreds of Hz, the microthrusters produce negligible jitter at frequencies above about 1 Hz.

To estimate the effect of roll of the telescope around the center of the WHC, assume that the reference stars are on a 2 arc minute diameter circle. The camera pixel scale is 17 mas in the infrared and the flux is sufficient to obtain 1/10th pixel accuracy. The angular resolution is then the pixel scale/ circle radius/10 = 2.8e-5 radian = 5.8 arc sec. The resulting on-sky tilt angle *dr* shown in Figure 6 is 29 mas, a pointing error larger than the PSF diameter. Even though this tilt is corrected by the coronagraph FSM, significant degradation in the wavefront would be expected because of the internal beam walk on M3 and the fold, before the beam reaches the FSM.

Consider now a larger FGS with 0.3 degree diameter FOV, modeled somewhat on the Hubble FGS. The Hubble sensor has an annular field of view surrounding the science fields, divided into three parts and covering 0.054 square degrees. Referring to Figure 3 showing the HabEx tertiary mirror, two sectors are placed on the annular fields of the TMA and each

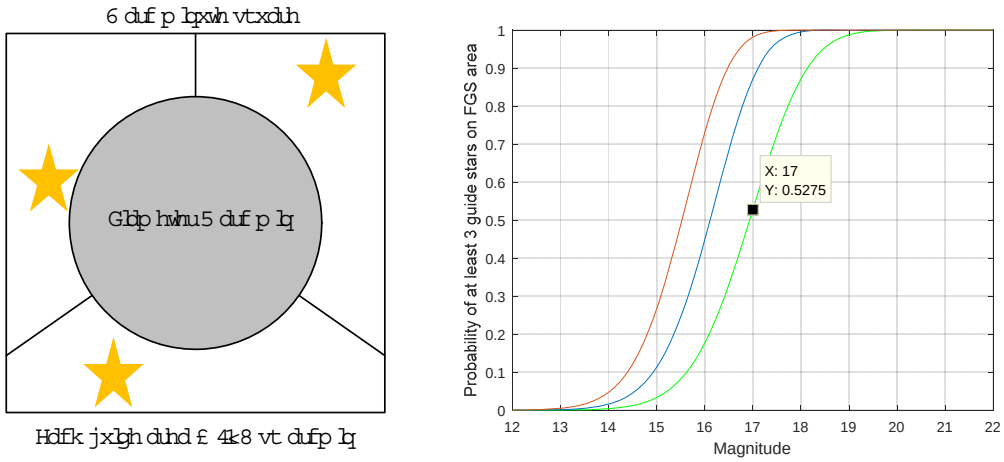

Figure 7: Left, three guide stars on outer part of WHC detector plane. Right, probability of three guide stars, (curves from left to right) red: on whole WHC area, blue: anywhere in outer area, green: one in each section of the outer area.

divided into two parts. A guide star is selected from three (or all) of the four sectors. The telescope is assumed to rotate about the center of these sectors, ie. near the center of the telescope FOV. With the same assumptions but with angle 0.15° between coronagraph FOV and FGS centers, the angular resolution is now 3.1e-6 radian = 0.65 arc sec. The resultant on sky angle is now 1.7 mas. This 17-fold improvement arises from the larger effective diameter of the sensor and the reduced lever arm between the sensor and coronagraph FOVs. Table 3 summarizes these results.

Table 3: FGS roll sensitivity comparison.

	Small FGS	Large FGS	
Angular resolution	5.8	0.65	arc sec
Angular resolution	2.8E-05	3.2E-06	radian
Angle between FGS and coronagraph	0.29	0.15	degrees
On-sky angle	29.6	1.70	mas

Fine Guidance Sensor Summary

A stellar magnitude of 17 or better is needed to establish 2 mas pointing accuracy at 100 Hz frame rate. Using microthrusters for attitude control should allow lower frame rates and hence fainter guide stars. A minimum of 3 guide stars is desirable to establish a reference orientation and the requirement for the probability of having 3 well separated stars was assumed to be ≥ 98%.

The Workhorse camera itself is an adequate detector for pointing the telescope 98% of the time. However it is inadequate for roll because there are too few well-separated stars and it has poor angular resolution around the line of sight. Also, although it is some distance away from the coronagraph field, it cannot practically be moved more than a factor of about two closer without changing the overall telescope design. Using a slower integration time on Workhorse camera does not help because of the poor angular resolution.

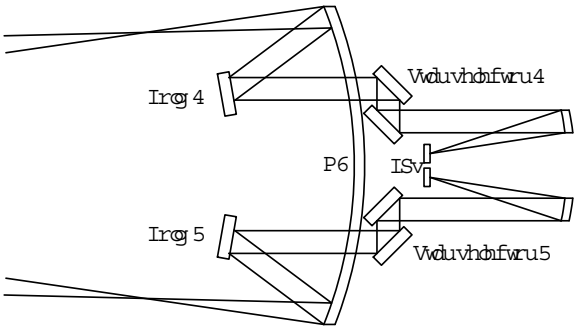

Figure 8: Dedicated FGS concept showing two of four beam paths.

The angular accuracy requirements depend particularly on: 1) the surface quality on the mirrors that experience most beam walk, in this case M3 and the fold mirror, 2) the accuracy of the estimate of the PSF center and 3) the availability of bright guide stars. Current technology allows the production of extremely well figured optics for UV lithography with 1 nm rms surface figure error. The contrasts given above assume this level of figure. For better centroid estimation, more total photons flux are required, implying a longer integration time. Going from 100 Hz frame rate to 10 Hz frame rate would yield a factor ~3 improvement in centroid accuracy, but the guide star count would still be low, yielding only 58% sky coverage. Therefore, an FGS working from sensors covering more widely spaced and wider fields is needed to control the roll to levels suitable for coronagraphy.

Dedicated FGS layout concept

A dedicated FGS can be built by utilizing some of the unused well-corrected annular field of the TMA. The FGS area on M3 is divided into 4 regions, separated at fixed fold mirrors and directed to field selector mirrors. These mirrors, situated at pupil planes are actuated to direct light from specific stars to a single focal plane or separate focal planes. Figure 8 shows the layout in concept, illustrating with just two FGS sensors. Each star selector places the brightest available guide star on its own focal plane. A set of four small sensors can be read out rapidly if necessary to accommodate brighter guide stars.

5. STARSHADE ACQUISITION

The starshade flies between 69,000 and 176,000 km away from the telescope, depending on the chosen science spectral band. In the nominal position when 'visible' light from 300 to 1000 nm is to be observed, the starshade range is 124,000 km. A high suppression shadow region exists behind the starshade and the telescope can move laterally ±1 m within the shadow without compromising the attenuation of the starlight. For the HabEx starshade design, the tips of the starshade are at an angle of 60 mas from the line of sight when the telescope is at the correct range and operating in the visible band; this angle is the inner working angle (IWA). The HabEx concept starshade is of the numerically optimized type, producing a defined high suppression wavelength band. Light of both shorter and longer wavelengths is attenuated but leaks into the shadow region and may be used for guiding. When performing science at longer wavelengths "red", shorter wavelength "blue" light is used for guiding, and vice versa. At the entrance pupil of the telescope, the shadow has some spatial structure, typically with a much diminished spot of Arago (or Poisson spot) at the center. The lateral position of the telescope within the shadow is sensed by imaging this structure onto a guide channel camera. The shadow structure is compared with a library of expected images to detect any

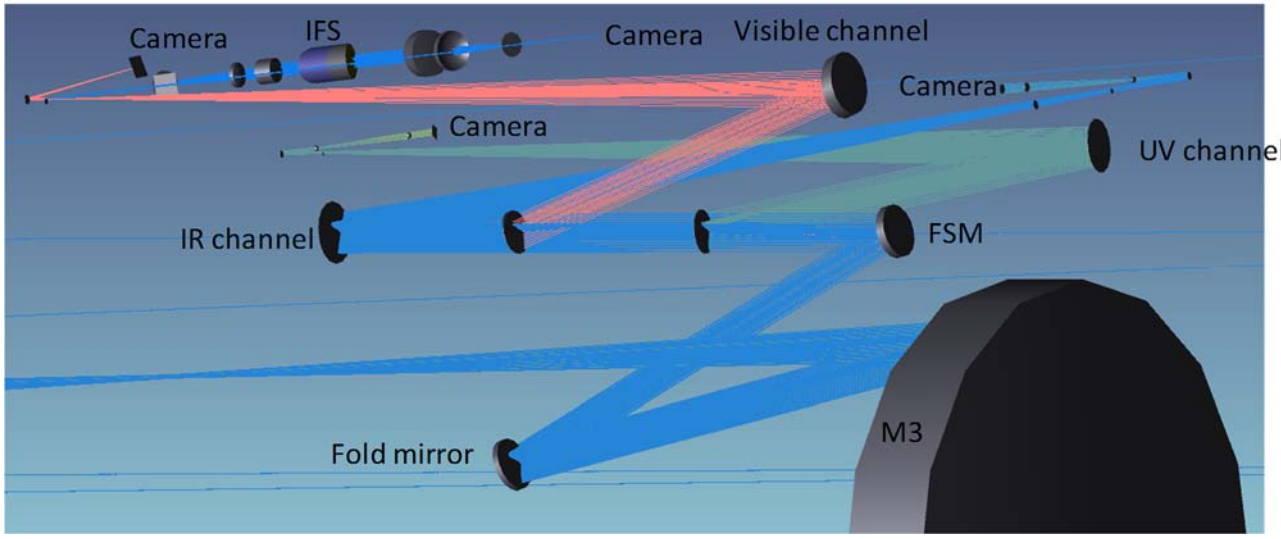

Figure 9: Starshade instrument. UV and IR channels have 'guide' modes allowing detection of starshade position by forming an image of the telescope pupil on the camera. The resulting image contains a predictable intensity structure which moves across the pupil as the starshade moves, allowing determination of the starshade's lateral position

starshade lateral offset from the line of sight to the star. Data on the offset are sent to the starshade and when the offset reaches the edge of the allowed area, thrusters are fired to effect repositioning. This general starshade guiding concept has been discussed elsewhere [12, 13, 14] and is the one now planned for the WFIRST-CGI starshade ready concept [15]. On WFIRST-CGI the existing low order Zernike wavefront sensor camera is used as a pupil plane imager, but the usual coronagraphic mask having the Zernike phase dimple is replaced by a plain dichroic.

Starshade Instrument

The starshade instrument (Figure 9) contains three independent channels: ultraviolet, visible and infrared. The UV and infrared channels each have a guide camera mode that projects a pupil image onto the focal plane. The visible channel carries a broadband integral field spectrograph (IFS) capable of covering the wavelength range from 450 to 1000 nm. The UV channel then covers the wavelengths from 450 nm down to 150 nm. The infrared and UV channels also carry spectrographs, a simple grism with R =7 for UV with slits to limit the field of view, and an IFS with R=40 for the IR.

Starshade acquisition

Between targets, the starshade must move across the sky to be ready to intercept the next target. The repositioning maneuver may take several days and at the end of the maneuver, the starshade must be located and brought onto the line of sight between the telescope and target star. The starshade carries a laser beacon bright enough to be detected alongside the bright target star. Initial acquisition of the starshade is performed on the WHC (see Table 4) which has a field of view of 3'x3', equivalent to a field between 60 and 154 km wide at the starshade range. With the 4 m telescope aperture, the position resolution (calculated as λ/d) is ~16 m, but in fact the starshade position can readily be determined at the sub pixel level to 2 m or so (calculated as $\lambda/d/\sqrt{N}$ where N is the number of photons from the star). This resolution improvement with photon count fails at large values of N where effects such as intra-pixel variation of quantum efficiency and uneven pixel spacing dominate, but determination to $1/10^{th}$ of the pixel is routine, while determination to $1/100^{th}$ of a pixel or better is possible with calibration of the focal plane [16]. When the starshade comes within ~4 km to ~10 km, depending on range, the telescope slews to locate the target star in the starshade camera's field of view and the starshade beacon is reacquired. Since slews are relatively slow, the starshade keeps moving while the slew takes place. Once slewed, the starshade instrument picks up the starshade location and will be ready for the next stage of fine guiding with the starshade partially or fully covering the star. The telescope pointing is controlled by the telescope's fine guidance system, so that at the starshade distance the pointing variation is typically less than ~0.5 m.

Table 4: Fields of view and starshade position resolution on the Workhorse and starshade cameras

Range (km)	WHC FOV size (km)	SSC FOV size (km)	PSF diameter λ/d (m) at 532 nm	Position resolution (m)
69000	60	1.97	9.18	0.9
124000	108	3.55	16.49	1.6
176000	154	5.03	23.41	2.3

When the starshade is some distance away from the star, the two sources, star and beacon, are imaged as distinct points of light, but as they close, especially when the star is much brighter than the beacon, then the starshade may be difficult to locate against the bright star. For this reason a flashing beacon is preferred so that a lock-in technique can be used. With the beacon on and then off, the distance between the two sources may be found. For very bright stars the starlight can be reduced in intensity by inserting a narrow bandpass filter, without affecting the laser beacon intensity. For example, if the star is ten times brighter than the beacon, and the two are close together, the effect of motion of the beacon on the centroid position of the beacon + starlight is diminished by a factor of ten. This effect can be minimized by attenuating the starlight appropriately.

The PSF size corresponds to a distance of 16 m (assuming a 532 nm laser wavelength) at a distance of 124,000 km (Table 4). The positional resolution limit is ~ 16 meters/SNR or 1.6 m in this case, taking a conservative estimate. The differential lateral offset accuracy between the star and the starshade will be ~1.4× worse than this. Table 4 shows the approximate starshade position resolution during acquisition, assuming a signal to noise ratio of 10 for the three starshade working ranges. Assuming a 20 W laser on the starshade with the beam diverging at a 1° full angle, counts of ~10^8 photoelectrons are achieved in exposure times of 1 second. A sun-like star at 10 pc will produce ~10^9 photoelectrons/s. Both fluxes are more than enough to saturate the detector, so a neutral density filter will cut down the flux to a suitable level. The SNR will be typically at least 100.

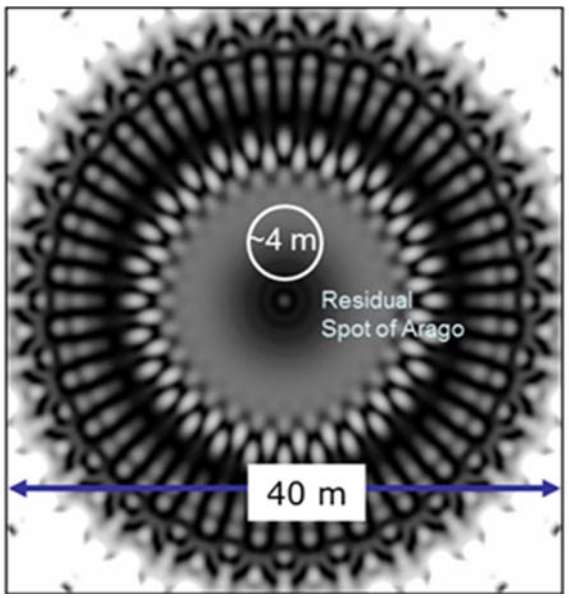

Figure 10: Starshade shadow in out of band light: light at wavelengths ~2x the longest science wavelength. The fine structure at the outer radii is created by the petals. Nearer the center, the pattern assumes a smooth circular symmetry and radial gradient and shows a residual spot of Arago at the center.

Starshade acquisition is therefore a process of moving from a dead-reckoning position calculated from the initial starting point and measurements of the starshade acceleration under the thruster firing, to optical determinations of the position relative to the target star. Once the starshade is found in the WHC FOV, trajectory corrections will direct it towards the target star and as it approaches more closely it will be progressively slowed to a few m/s so that when the telescope slew takes place it will be moving slowly across the starshade visible camera's FOV.

The starshade diameter is 72 m, so that the starlight begins to be obscured when the starshade is ~36 m off axis. As the starshade moves towards the line of sight, the starlight dims and at about 20 m off axis, the patterned edge of the starshade's shadow will be detectable on the starshade instrument's own guide camera. Typically, starshade designs form similar shadow patterns at the telescope working distance, varying in scale with the starshade. Figure 10 shows a logarithmic plot of the shadow pattern for a starshade designed for WFIRST and rescaled to HabEx dimensions. The shadow varies in intensity by about four orders of magnitude between the edge and the center.

At this point in the formation acquisition process, the starshade beacon is switched off and final alignment proceeds on the guide camera operating in pupil mode. To do this, an optic is inserted into the camera path which switches the camera from imaging the sky to forming an image of the telescope entrance pupil. Initially, the starshade shadow has a strong gradient which can be followed to guide the starshade onto the line of sight. As the starshade becomes better centered over the star, the guidance method switches to pattern-based matching against the calculated shadow pattern. In this mode, the positioning problem is easier since the scale of features in the shadow is driven by the wavelength divided by the starshade size. With that scale being ~0.7 m, given sufficient stellar leakage flux the starshade position can be readily determined to 1/10th of this. Thus, the starshade position can be accurately measured once in place, and maintained within the ±1 m design envelope.

6. CONCLUSION

Pointing for HabEx requires a fine guidance sensor with a field of view reaching across the TMA telescope's innate annular field. This requirement derives from the need to measure telescope roll to high precision, in turn preventing excessive beam walk in the coronagraph beam train. An accurate sensor is not in itself sufficient; excellent surface quality (~ 1 nm rms) is needed on the part of the telescope tertiary mirror that the coronagraph beam intercepts, but this requirement is within the state of the art.

Good telescope pointing stability also relies on control of the position of the internal optics M1 through M3 and this is achieved using a laser metrology system driving a set of actuators to keep M2 and M3 in position relative to M1. Such control is not need at high bandwidth, because the telescope carries no reaction wheels which create high frequency

vibration. Instead, the telescope is pointed using microthrusters which produce negligible disturbance at frequencies higher than 1 Hz.

Starshade acquisition relies on methods similar to those baselined in concept studies for WFIRST. In this case, the relatively wide field of the workhorse camera is used for initial acquisition, passing to the starshade camera for final approach. Once within 20 m or so of the line of sight, the starshade position is accurately measured using the pupil plane image of the starshade shadow.

ACKNOWLEDGEMENTS

The information in this paper is pre-decisional and is provided for planning and discussion purposes only. This work was conducted at the Jet Propulsion Laboratory, California Institute of Technology, under contract with the National Aeronautics and Space Administration.

REFERENCES

1. HabEx space telescope optical system, Stefan Martin, Mayer Rud, Daniel Stern, Paul Scowen, Joel Nissen, John Krist, Proc. SPIE. 10398, 2017.

2. Overview of a telescope concept design for the Habitable-zone Exoplanet Direct Imaging Mission, H. Philip Stahl, Proc. SPIE. 10398, 2017.

3. Wavefront sensing for a future HabEx space telescope, Joel Nissen and Stefan Martin, Adaptive Optics for Extremely Large Telescopes, 2017.

4. PROPER: an optical propagation library for IDL, John E. Krist, Proc. SPIE 6675, 2007.

5. Have confidence in your coronagraph: statistical analysis of high-contrast coronagraph dynamics error budgets, Marie Levine, Stuart Shaklan, Luis Marchen, Lee Peterson, Proc. SPIE. 9150, 2014

6. Fine guidance sensors aboard the Hubble Space Telescope: the scientific capabilities of these interferometers, Russell Makidon, Lauretta Nagel, Larry Wasserman, Olivia Lupie, G. Benedict, Edmund Nelan, Barbara McArthur, Linda Abramowicz-Reed, Otto Franz, Proc. SPIE. 3350, 1998.

7. Optical design of the JWST fine guider sensor, Clinton Evans and Sheng Hai Zheng, Proc. SPIE. 7786, 2010.

8. Wide Field Camera 3 Instrument Handbook for Cycle 24, STSCI 3700 San Martin Dr., Baltimore, MD 21218.

9. http://spacemath.gsfc.nasa.gov

10. Dynamic testbed demonstration of WFIRST coronagraph low order wavefront sensing and control (LOWFS/C), Fang Shi, Xin An, Kunjithapatham Balasubramanian, Eric Cady, Brian Kern, Raymond Lam, David Marx, Camilo Mejia Prada, Dwight Moody, Keith Patterson, Ilya Poberezhskiy, Byoung-Joon Seo, Joel Shields, Erkin Sidick, Hong Tang, John Trauger, Tuan Truong, Victor White, Daniel Wilson, Hanying Zhou, Proc. SPIE. 10400, 2017.

11. Colloid Microthruster Feed System Development for Fine Pointing and Drag-Free Control of Multi-Year Astronomical Observatories, Ziemer, John, Mueller, J., Spence, D., Hruby, V., AAS Meeting #223, January 2014

12. Precise starshade stationkeeping and pointing with a Zernike wavefront sensor, Michael Bottom, Carl Seubert, Shannon Kian Zareh, Stefan Martin, Eric Cady, Stuart Shaklan, Proc. SPIE. 10400, 2017.

13. Alignment of a terrestrial planet finder starshade at 20-100 megameters, Martin Charles Noecker, Proc. SPIE. 6693, 2007.

14. Enabling Formation Flying of Starshades for the Search of Earth-Like Exoplanets, Anthony Harness, IWSCFF-2015.

15. Optical instrumentation for science and formation flying with a starshade observatory, Stefan Martin, Eric Cady, Daniel Scharf, Hong Tang, Carl Liebe, Proc. SPIE. 9605, 2015.

16. Micro-pixel accuracy centroid displacement estimation and detector calibration, Chengxing Zhai, Mike Shao, Renaud Goullioud and Bijan Nemati. Proc. Royal Society: Mathematical, Physical and Engineering Sciences, Vol. 467, No. 2136 (8 December 2011), pp. 3550-3569.

BIOGRAPHY

Stefan Martin *is a Senior Optical Engineer at the Jet Propulsion Laboratory in Pasadena, Ca. He received a B.Sc. in Physics from the University of Bristol in the UK and a PhD in Engineering from the University of Wales. At JPL, he has been leader of the TPFI Flight Instrument Engineering Team, Testbed Lead for the TPFI Planet Detection Testbed and is currently Payload Lead for the HabEx telescope design study. He was optical engineer for the Exo-S starshade study and has developed possible methods for implementing starshades on future space telescopes such as WFIRST.*